Massive Stars Near and Far
Proceedings IAU Symposium No. 361, 2024
J. Mackey, J. S. Vink, & N. St-Louis, eds.
doi:10.1017/S1743921322002885

Two-dimensional models of fast rotating stars and mixing processes

Michel Rieutord[1] **and Damien Gagnier**[2]

[1]IRAP, Université de Toulouse, CNRS, UPS, CNES, 14, avenue Édouard Belin, F-31400 Toulouse, France
email: mrieutord@irap.om.eu

[2]Institute of Theoretical Physics, Faculty of Mathematics and Physics, Charles University, V Holešovičkách R, Prague 8, 18000, Czech Republic
email: damien.gagnier@mff.cuni.cz

Abstract. In this short review we present the recent progresses in modelling fast rotating stars in two dimensions. We thus give a brief description of the features of the public domain code ESTER that can compute self-consistently the structure and the large-scale flows (differential rotation and meridional circulation) of an axisymmetric stellar model of a (fast) rotating early-type main sequence star. We illustrate these modelling with the recent results obtained on Altair, a nearby extremely fast rotator. We then discuss the various way mixing takes place in the stably stratified radiative envelope of early-type stars, and especially in massive ones where the radiative winds add a new source of large-scale flows, which are shown to be strongly anisotropic and very difficult to represent in one dimension.

Keywords. Rotation, early-type stars, spin-down

1. Introduction

As far as massive stars are concerned, rotation is a concern! Why? Massive stars are intrinsically young objects and their formation fueled them with a lot of angular momentum, so much that most of the time they are members of binary or multiple systems. Making a binary is indeed an efficient way to store angular momentum. Hence, the fact that massive stars are almost never alone may be interpreted as a signature of a formation process that provides the stars with a high amount of angular momentum. Hence, it is no surprise that fast rotation is commonly detected among massive stars.

The foregoing considerations have motivated several extended observational studies to measure the impact of rotation in the population of O-type stars (Ramírez-Agudelo *et al.* 2013, 2015; Holgado *et al.* 2022). From these studies it turns out that the initial rotation velocity of O-type stars is around 20% of the break-up rotational velocity. Binarity and strong winds may be reasons for this not so fast rotation. But if we now consider B-type stars which typically cover the low mass end of massive stars (i.e. from 3 $M_\odot$ to ~ 20 $M_\odot$), the work of Huang *et al.* (2010) shows that $\sim 45\%$ of galactic B-type stars have a $V \sin i \gtrsim 150$ km/s, while still 30% of these stars show a $V \sin i \gtrsim 200$km/s. This latter fraction is even higher in the Large Magellanic Cloud, presumably because of its lower metallicity (e.g. Dufton *et al.* 2013).

Two well studied stars illustrate fast rotation of massive stars:

- ζ Ophiuchi of type O9.5, thus near the upper limit of B-type stars, has a $V \sin i \simeq 400$ km/s (Kambe *et al.* 1990).
- ϕ Persei of type B2 has a $V \sin i \simeq 450$ km/s (Poeckert 1981).

For both of these stars, centrifugal effect is quite significant: Repolust *et al.* (2004) indicate that the mass of ζ Oph is around 20 $M_\odot$ and that its radius (assumed a polar radius) is $R \simeq 8.9\ R_\odot$. With a minimum equatorial velocity of 400 km/s, the Roche model gives a flattening

$$\varepsilon = 1 - \frac{R_p}{R_{\rm eq}} = \frac{R_p V_{\rm eq}^2}{2GM} \simeq 0.16$$

where R_p and $R_{\rm eq}$ are the polar and equatorial radii respectively. $V_{\rm eq}$ is the equatorial velocity, G the gravitation constant and M the mass of the star.

The same exercise applied to ϕ Per, with a mass $M \simeq 9.6\ M_\odot$ (Schootemeijer *et al.* 2018), a polar radius of 5.5 $R_\odot$ and an inclination $i = 80°$ (Gies *et al.* 1998), we get a flattening $\varepsilon \simeq 0.24$.

Such flattened stars obviously require two dimensional models if all the effects of fast rotation are to be taken into account properly.

2. Two-dimensional stellar models

2.1. *The ESTER code*

By 2D stellar models we understand models where the sole symmetries are axisymmetry and symmetry with respect to the equatorial plane. Hence, all quantities describing the stellar structure like pressure or density, or describing large-scale flows, namely differential rotation and meridional circulation, only depend on the spherical coordinates (r, θ). Moreover, they are invariant in the transform $\theta \to \pi - \theta$ (equatorial symmetry).

Any self-consistent 2D model should include the aforementioned large-scale flows. The main flow is the differential rotation, which is driven by the baroclinic torque. Let us recall the origin of these motions. If we consider the momentum equation, written in a galilean frame, it reads:

$$(\vec{v} \cdot \vec{\nabla})\vec{v} = -\frac{1}{\rho}\vec{\nabla}P - \vec{\nabla}\phi_g + \frac{1}{\rho}\vec{F}_{\rm visc} \tag{2.1}$$

for a steady state. In this equation ϕ_g is the gravitational potential and $\vec{F}_{\rm visc}$ the viscous force. Outside boundary layers (or shear layers), the viscous force is negligible and therefore we leave it aside. Since we assume that the model is axisymmetric, the velocity field $\vec{v}$ reads:

$$\vec{v} = r \sin\theta\, \Omega(r,\theta)\vec{e}_\varphi + v_r(r,\theta)\vec{e}_r + v_\theta(r,\theta)\vec{e}_\theta.$$

Here, $\Omega(r,\theta)$ is the differential rotation, while (v_r, v_θ) stand for the components of the meridional circulation. Now, taking the curl of the momentum equation and neglecting the viscous force, yields the so-called thermal wind equation, well-known in atmospheric physics (see Cushman-Roisin 1994, for instance),

$$r \sin\theta \frac{\partial \Omega^2}{\partial z} = \frac{\vec{\nabla}P \times \vec{\nabla}\rho}{\rho^2} \cdot \vec{e}_\varphi \tag{2.2}$$

which shows that the non-alignment of the density and pressure gradients, generates a torque, the so-called baroclinic torque, that forces a gradient of the angular velocity Ω along Oz, the rotation axis direction. The non-alignment of these two gradients results from the fact that pressure and temperature obey two independent equations. Further details on the dynamics of 2D models may be found in Espinosa Lara & Rieutord (2013).

https://doi.org/10.1017/S1743921322002885 Published online by Cambridge University Press

The full problem to be solved for the construction of an axisymmetric model of a fast rotating star is actually given by the four partial differential equations:

$$\begin{cases} \Delta\phi = 4\pi G\rho \\ \rho T\vec{v}\cdot\vec{\nabla}S = -\mathrm{Div}\vec{F} + \varepsilon_* \\ \rho(2\vec{\Omega}_*\wedge\vec{v} + \vec{v}\cdot\vec{\nabla}\vec{v}) = -\vec{\nabla}P - \rho\vec{\nabla}(\phi - \frac{1}{2}\Omega_*^2 s^2) + \vec{F}_{\mathrm{visc}} \\ \mathrm{Div}(\rho\vec{v}) = 0. \end{cases} \tag{2.3}$$

where we recognise Poisson equation, the entropy equation, the momentum equation (here written in a frame rotating at the angular velocity $\vec{\Omega}_*$), and the mass conservation equation. For fluid dynamicists these equation are those of a compressible, self-gravitating fluid harbouring nuclear heating $\varepsilon_*(\rho, T)$. These partial differential equations are completed by the equation of state $P \equiv P(\rho, T)$, the expression of the heat flux $\vec{F}$ and boundary conditions. These latter conditions apply at the surface of the star and at the centre. At the centre, we just demand that the functions be regular, while at the surface the pressure, the velocity and the temperature should meet appropriate conditions depending on where we stop the modelling. A classical one (see Espinosa Lara & Rieutord 2013), is to fix the surface at the optical depth $\tau = 2/3$, where we set the pressure and the heat flux as a black body radiator. In two dimensions we also need to give boundary conditions on the velocity field. At the centre, regularity and axisymmetry impose a zero-velocity while at the surface it is natural to impose stress-free conditions if we neglect any wind (see below). In a steady state, such conditions generate a weak Ekman layer which determines a weak meridional circulation and insures a neat zero-flux of angular momentum across any closed surface inside the star. Of course, if some region of the star is turbulent, $\vec{F}$ and $\vec{F}_{\mathrm{visc}}$ should be completed with the appropriate turbulence model.

The above equations form a rather formidable nonlinear problem, which has been solved for the first time by Espinosa Lara & Rieutord (2013) using a simple turbulence model. The way to reach the numerical solution is detailed in Rieutord *et al.* (2016). Very briefly, it uses the three following items:

- A mapping to follow the star distortion,
- A spectral method (Chebyshev polynomials and spherical harmonics),
- The Newton-Raphson algorithm.

The code where this solution is implemented is the public domain ESTER code that may be obtained on GitHub at `http://ester-project.github.io/ester/`. Presently, this code works well for early-type stars, but still needs developments for late-type stars. The quality of the solutions are gauged with the energy and virial tests, namely two integrals that should be vanishing if the solution is exact. The virial test requires that

$$\int_{(V)} \vec{r}\cdot\left[2\vec{\Omega}\wedge\rho\vec{u} + \rho\vec{u}\cdot\vec{\nabla}\vec{u} + \rho\vec{\nabla}\phi - \rho\Omega^2 s\vec{e}_s - \mathbf{Div}[\sigma]\right] dV = 0$$

where $[\sigma]$ is the viscous stress tensor. The foregoing integral is normalized by the potential energy,

$$W = \frac{1}{2}\int_{(V)} \rho\phi\, d^3\vec{r}.$$

This test usually leads to errors less than 10^{-9} thanks to the spectral discretization. The energy test, which compares the energy produced by nuclear reactions and the energy emitted at the surface, is not as good because of rapid variations (and the tabulated nature) of opacities near the stellar surface.

https://doi.org/10.1017/S1743921322002885 Published online by Cambridge University Press

Table 1. Fundamental parameters of Altair according to Bouchaud *et al.* (2020). The luminosity has been calculated using the same model as Bouchaud *et al.* (2020). The distance is the one given by Hipparcos (van Leeuwen 2007).

Star	Spectral type	Distance pc	Mass $M_\odot$	R_{eq} $R_\odot$	R_{pol} $R_\odot$	T_{eq} K	T_{pol} K	Lum. $L_\odot$
α Aql	A7 IV-V	5.130 ±0.015	1.86 ±0.03	2.008 ±0.006	1.565 ±0.014	6780	8620	10.2
Flattening	Ω_{eq}/Ω_k	*incl.* deg	V_{eq} km/s	P_{eq} day	$X_{env.}$	X_{core}	Z	
0.220 ±0.003	0.744 ±0.01	50.65 ±1.23	313 ±9	0.325 ±0.01	0.733	0.71	0.019	

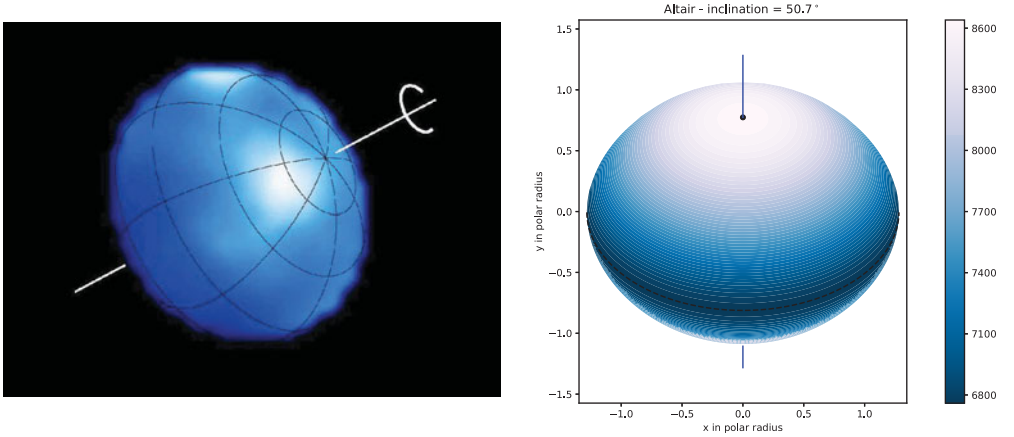

Figure 1. Left: Altair as seen with the CHARA interferometer at Mount Wilson (credit Monnier *et al.* 2007). Right: Distribution of the effective temperature at the surface of Altair's model by Bouchaud *et al.* (2020).

2.2. *Altair's test case*

Altair is a nearby intermediate mass star that is rotating very rapidly (see Tab. 1 for a recap of Altair's fundamental parameters). Because of its proximity, this star has been observed in many ways, notably with interferometers (CHARA at Mount Wilson see Fig. 1, PIONIER and GRAVITY at ESO-Chile) to measure its oblateness. Dedicated spectroscopy determined its $V \sin i$ with constraints on i, the inclination of the rotation axis over the line of sight (see Reiners & Royer 2004), while asteroseismology also brought its contribution to the set of data with a small set of identified acoustic frequencies showing delta-scuti-type oscillations (see Buzasi *et al.* 2005; Bouchaud *et al.* 2020; Le Dizès *et al.* 2021).

This abundant data set motivated Bouchaud *et al.* (2020) to devise a concordance model of Altair that matches all known observables. We show in Fig. 1 the effective temperature distribution that is used to retrieve spectroscopic and interferometric observables.

At the same time the matching between model and data shows us that ESTER models can give a faithful representation of real fast rotating early-type stars. Accompanied with the TOP code (Reese *et al.* 2021), which can compute the eigenmodes of an ESTER model, the main conclusion of Bouchaud *et al.* (2020) was that the mass of Altair is 1.86 ± 0.03 $M_\odot$ and that it is a young star, namely ∼100 Myrs old, unlike previous estimates based on 1D models.

https://doi.org/10.1017/S1743921322002885 Published online by Cambridge University Press

3. Rapidly rotating massive stars

3.1. *Introduction*

Altair is by far not a massive star! According to Langer (2012) a massive star is "a star that is massive enough to form a collapsing core at the end of its life and, thus, avoid the white dwarf fate". Hence, the minimum mass is in between 8 and 12 $M_\odot$, depending on metallicity. The final fate of massive stars is a full research field by itself, which is however strongly connected to what happens in the early phases of evolution, especially during the main sequence (see Martins & Palacios 2013). Here, we shall focus on this main sequence stage and review the recent progresses brought by 2D-models.

Compared to Altair and intermediate mass stars, massive stars own a new feature, such as a non-negligible mass-loss. This mass-loss is driven by the strong radiation field at the surface of the star and as far as rotation is concerned, we may anticipate two effects: (i) a lower critical angular velocity due to radiative acceleration, (ii) an intensified mixing due to the spin-down associated with angular momentum losses.

3.2. *Critical angular velocity*

When the radiation field is intense, the radiative acceleration is a non-negligible part of the forces applied to a fluid element. At some height in the atmosphere this acceleration dominates and the wind is launched. However, in the lower parts of the photosphere, where the outflow is largely subsonic, radiative acceleration may help decrease the critical angular velocity over which equatorial surface matter is just orbiting the star.

This question was first investigated by Maeder (1999) and Maeder & Meynet (2000) using 1D models. Since the use of 1D-models gives rather uncertain results when one considers rotation near the critical one, Gagnier *et al.* (2019a) reconsidered this issue in light of 2D-models.

Critical angular velocity is reached when, somewhere at the surface of the star the total acceleration vanishes, namely

$$\vec{g}_{\rm tot} = \vec{g}_{\rm eff} + \vec{g}_{\rm rad} = \vec{0} \tag{3.4}$$

where $\vec{g}_{\rm eff}$ is the effective gravity (the combination of gravity and centrifugal acceleration). Since the radiative acceleration $\vec{g}_{\rm rad}$ is proportional to the radiative flux, namely $\vec{g}_{\rm rad} = \kappa\vec{F}/c$, where κ is a mean opacity weighted by the flux, we immediately see that a vanishing total acceleration is reached if the flux reaches the limit $\vec{F}_{\rm lim} = -c\vec{g}_{\rm eff}/\kappa$. Then, it is usual to introduce the Eddington factor as the ratio

$$\Gamma_\Omega(\theta) = \frac{F}{F_{\rm lim}}$$

and note that

$$\vec{g}_{\rm tot} = \vec{g}_{\rm eff}(1 - \Gamma_\Omega(\theta))$$

where the Eddington factor obviously depends on the rotation rate, because of the centrifugal acceleration, and on the colatitude θ because of the gravity darkening induced by the centrifugal distortion of the star.

Gagnier *et al.* (2019a) used the ω-model of Espinosa Lara & Rieutord (2011), which assumes that the flux in a radiative envelope is just anti-parallel to the effective gravity (but see also Rieutord 2016). This models is very close to complete 2D-models and allows a simple analysis of this problem. The main results, confirmed by the full 2D-models, are that:

- the critical angular velocity is always reached at equator, in line with the results of the first investigations of Maeder & Meynet (2000),

https://doi.org/10.1017/S1743921322002885 Published online by Cambridge University Press

- the critical angular velocity reads

$$\Omega_c = \Omega_k \sqrt{1 - \Gamma_{eq}^{3/2}} \ . \tag{3.5}$$

where Ω_k is the Keplerian angular velocity at equator. 1D-models lead to a slightly different law $\Omega_c \propto \sqrt{1-\Gamma_{eq}}$ if $\Gamma \geq 0.639$ and $\Omega_c = \Omega_k$ otherwise, which shows a stronger impact of $\vec{g}_{\rm rad}$ than (3.5).

Actually, the investigations by Gagnier *et al.* (2019a), show that the decrease of opacity with density, still reduces the impact of the radiative acceleration on the critical angular velocity. Gagnier *et al.* (2019a) conclude that below 40 $M_\odot$ Ω_c and Ω_k differ only very slightly.

3.3. *Evolution with mass-loss*

To follow the evolution of a mass-losing star, and especially to follow its rotation rate, one usually peels off the star: some amount of mass is removed with the angular momentum it contains, assuming it comes from the surface layers. Gagnier *et al.* (2019b) used the same technique but applied to 2D-models. To be operative, one needs to know the mass-loss at each colatitude, namely the function $\dot{m}(\theta)$.

In a fast rotator, gravity darkening and centrifugal acceleration control the local radiative flux and the local effective gravity respectively. Hence, with metallicity, to which we may attribute a global value, we need to derive the dependence of the local mass flux $\dot{m}(\theta)$ with respect to the local effective temperature and gravity. Gagnier *et al.* (2019b) devised such a relation based on the works of Castor *et al.* (1975), Pauldrach *et al.* (1986) and Vink *et al.* (1999, 2001), mainly. In particular, the work of Vink *et al.* (1999) noticed the bi-stability jump at $T_{\rm eff} \simeq$25,000 K in radiative winds of early-type supergiants and discovered that it is due to the growing importance of FeIII transitions at effective temperature below 25,000 K. Since the surface of fast rotating stars can support a large range of effective temperatures, thanks to gravity darkening, Gagnier *et al.* (2019b) logically found that such massive stars may be endowed with a two-winds regime: a slow and "cold" wind in the equatorial regions where effective temperatures are below the threshold, and a faster hotter wind near the poles. Not surprisingly, the slow equatorial wind is efficient at removing angular momentum of the star.

The foregoing wind processes lead to the following evolution of rotation in massive stars: As the star evolves (along the main sequence) and inflates, it gets closer to the critical rotation if mass-loss is weak enough. In a few words, this behaviour comes from the fact that as the star evolves, and loses a negligible amount of angular momentum, its rotation rate decreases because of radius expansion, however the Keplerian angular velocity at equator decreases even more, hence the ratio $\omega = \Omega_{\rm eq}/\Omega_k$ increases with time. If the initial angular velocity is large enough the star may reach the critical rotation within the main sequence. However, the wind may modify this evolution. If we consider a star whose initial effective temperature is above 25,000K, it will lose mass in a single wind régime. In addition, mass-loss is stronger at the pole because of gravity darkening. But around the pole angular momentum loss is weak and the star actually follows a route similar to the no-mass-loss case. However, at some time gravity darkening can be strong enough to put the equatorial effective temperature below the threshold and a two winds régime starts. Here the angular momentum loss is much more efficient and the star can move away from criticality. This scenario is illustrated in Fig. 2 taken from Gagnier *et al.* (2019b).

3.4. *Interior flows*

The peeling off process is valid as long as the mass-loss timescale is longer than the timescale of angular momentum transfer inside the star. As shown in Gagnier *et al.* (2019b) (see their Tab. 1), this is quite the case for stars up to 20$M_\odot$.

https://doi.org/10.1017/S1743921322002885 Published online by Cambridge University Press

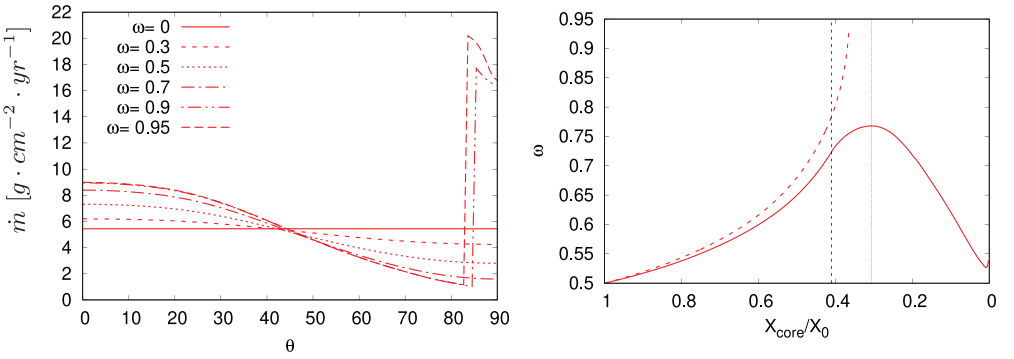

Figure 2. Left: the surface mass flux as a function of colatitude for various rotation rates scaled to the critical one (Gagnier *et al.* 2019a). Right: Evolution of rotation rate scaled by the critical angular velocity according to Gagnier *et al.* (2019b) for a mass-losing model (solid line) and a no-mass-loss model (dashed line); time is represented by the hydrogen mass fraction in the convective core scaled by its initial value. For both figures a 15 $M_\odot$ model is used.

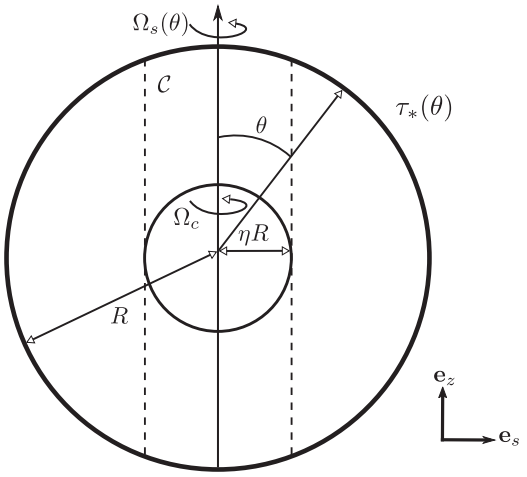

Figure 3. Set-up used to study the internal motion of a fluid in a spinning-down spherical shell braked by a shear stress.

However, this spin-down process also induces some mixing inside the star, which is still not well known. Gagnier & Rieutord (2020) thus investigated the steady flows that results from the spinning down star.

One part of the problem is the determination of the flow that results from the viscous stress generated by the out moving layers. To study the implications of this effect Gagnier & Rieutord (2020) first analysed the flow of a rotating fluid confined into a spherical shell representing the radiative envelope of a massive star. At its surface they imposed a stress of the form:

$$\sigma_{r\varphi} = \tau_*(\theta) = -A \sin\theta$$

which extract angular momentum from the fluid. The set-up is reproduced in Fig. 3.

In this set-up the core is rotating as a solid body and no-slip boundary conditions are used at its interface with the envelope. This is supposed to represent the viscosity jump at the core-envelope boundary. The convective core is endowed with a high viscosity that reflects the turbulent diffusion there (e.g. Rieutord 2006).

https://doi.org/10.1017/S1743921322002885 Published online by Cambridge University Press

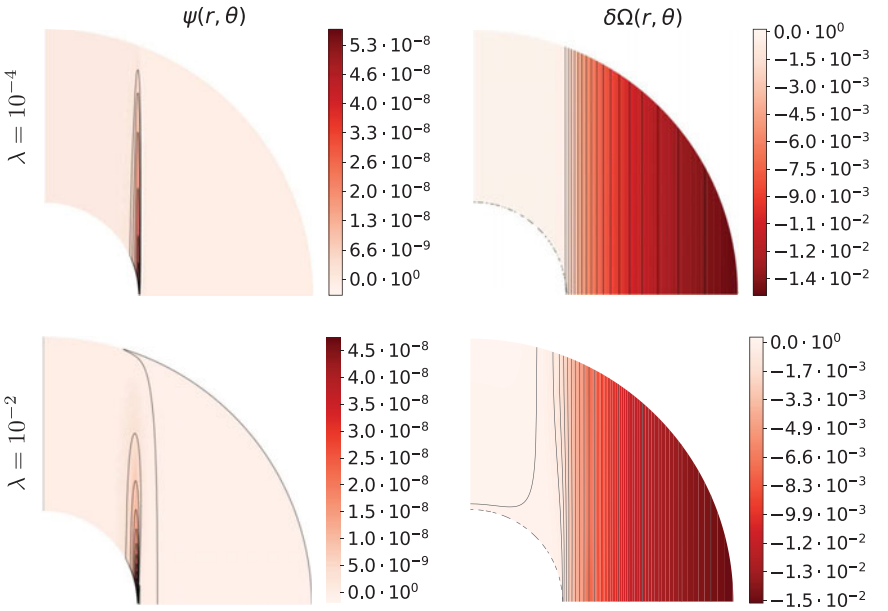

Figure 4. Meridional circulation (left) and differential rotation (right) generated in a spinning-down radially stably stratified spherical shell braked by a shear stress. The Ekman number is $E = 10^{-7}$ and the Boussinesq approximation is used (from Gagnier & Rieutord 2020).

The solution of this spin-down problem is shown in Fig. 4 with a meridional cut. There are two striking features characterizing these solutions. First, we note that the meridional circulation is concentrated in a thin shear layer that is tangent to the core, lying on the tangent cylinder. This layer is well known in the theory of rotating fluids as the Stewartson layer (e.g. Stewartson 1966). In Fig. 4, the fluid in the spherical shell is stably stratified radially, as in the actual radiative envelope. A stable stratification may actually inhibit the raise of a Stewartson layer, but Gagnier & Rieutord (2020) have found that this inhibition is controlled by the parameter

$$\lambda = \mathcal{P}\frac{N^2}{4\Omega^2}$$

where $\mathcal{P}$ is the Prandtl number and N the Brunt-Väisälä. A similar result was also found in previous work (Garaud 2002; Rieutord 2006). In stars, heat diffusion is large and this parameter is small when the star is rapidly rotating. Indeed, $N^2/4\Omega^2$ is less than 100 in fast rotating stars, while the Prandtl number $\mathcal{P}$ is of order of 10^{-6}. Hence, $\lambda \ll 1$ for these stars. In that case the role of stratification is negligible. Of course, if the star rotates slowly λ may be much larger than unity and in that case stratification suppresses the Stewartson layer (e.g. Gagnier & Rieutord 2020).

The Stewartson layer is a feature that is not taken into account in 1D models, while we see that it is linking the core and the surface of the star. Hence, it is able to carry elements from the deep interior to the surface where they may be observed.

The second feature that may be noticed in Fig. 4, is the concentration of the differential rotation in the outer part of the tangent cylinder. As far as the transport properties are concerned, we note that any turbulent transport sustained by the shear associated with the differential rotation is therefore confined outside the tangent cylinder. Moreover, as shown by Fig. 5, when the density stratification is taken into account, this same differential rotation, generated by the spin-down (or the surface stress actually), is now

https://doi.org/10.1017/S1743921322002885 Published online by Cambridge University Press

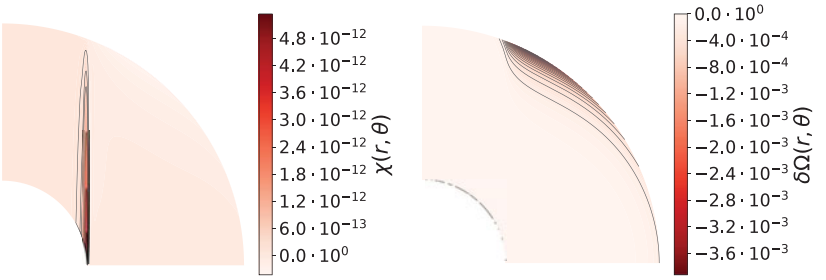

Figure 5. The same as in Fig. 4, but using the anelastic approximation with a density contrast between core and surface of 10^4.

confined in an even narrower region of the radiative envelope. It shows again that the transport properties in a radiative envelope are strongly anisotropic and inhomogeneous.

4. Conclusions and outlook

After this brief overview of the internal dynamics of rapidly rotating massive stars, we certainly feel that much work is ahead of us. Such stars indeed require two-dimensional models, not only because they are flattened by centrifugal effect but also because they own internal flows that strongly break the spherical symmetry. As a consequence, the way chemical elements and angular momentum is transported between the core and the envelope is quite far from what 1D model can predict.

We have seen that baroclinic and spin-down flows span the radiative envelope of these stars, but we should expect that magnetic fields also add their part of anisotropy. They have been detected in many sorts of massive stars like β Cephei or Be stars (Hubrig *et al.* 2011). As is well-known, winds and magnetic fields give rise to magnetic braking which is a strong effect, but of higher complexity since in such a problem the geometry generally loses any symmetry, leaving us with a 3D problem.

But before attacking the foregoing challenging problem, some simpler questions can be addressed with present 2D models. Let us point out three of them:

- The secular time evolution along the main sequence of a 2D-model including mass-loss and its coupling with the interior flows,
- the launch of matter near critical rotation,
- the role of Stewartson layers in the mixing process and the angular momentum transport at the core-envelope interface.

Acknowledgments

MR is very grateful to the organizers for their invitation to participate in this conference and especially to Jonathan Mackay for his kind reading of the manuscript. We also wish to thank the support of the French Agence Nationale de la Recherche (ANR), under grant MASSIF (ANR-21- CE31-0018-02). Numerical simulations have been made with HPC resources from CALMIP supercomputing center (Grant 2022-P0107).

References

Bouchaud, K., Domiciano de Souza, A., Rieutord, M., Reese, D. R., & Kervella, P. 2020, A&A, 633, A78

Buzasi, D. L., Bruntt, H., Bedding, T. R. *et al.* 2005, ApJ, 619, 1072

Castor, J. I., Abbott, D. C., & Klein, R. I. 1975, ApJ, 195, 157

Cushman-Roisin, B. 1994, An introduction to geophysical fluid dynamics (Paris: Prentice-Hall)

Dufton, P. L., Langer, N., Dunstall, P. R. *et al.* 2013, A&A, 550, A109

https://doi.org/10.1017/S1743921322002885 Published online by Cambridge University Press

Espinosa Lara, F., & Rieutord, M. 2011, A&A, 533, A43
— 2013, A&A, 552, A35
Gagnier, D., & Rieutord, M. 2020, J. Fluid Mech., 904, A35
Gagnier, D., Rieutord, M., Charbonnel, C., Putigny, B., & Espinosa Lara, F. 2019a, A&A, 625, A88
— 2019b, A&A, 625, A89
Garaud, P. 2002, MNRAS, 335, 707
Gies, D. R., Bagnuolo, J., William G. *et al.* 1998, ApJ, 493, 440
Holgado, G., Simón-Díaz, S., Herrero, A., & Barbá, R. H. 2022, in A&A, arXiv:2207.12776
Huang, W., Gies, D. R., & McSwain, M. V. 2010, ApJ, 722, 605
Hubrig, S., Ilyin, I., Schöller, M., Briquet, M., Morel, T., & De Cat, P. 2011, ApJ Lett., 726, L5
Kambe, E., Ando, H., & Hirata, R. 1990, Pub. Astron. Soc. Jap., 42, 687
Le Dizès, C., Rieutord, M., & Charpinet, S. 2021, A&A, 653, A26
Maeder, A. 1999, A&A, 347, 185
Maeder, A., & Meynet, G. 2000, A&A, 361, 159
Martins, F., & Palacios, A. 2013, A&A, 560, A16
Monnier, J. D., Zhao, M., Pedretti, E. *et al.* 2007, Science, 317, 342.
Pauldrach, A., Puls, J., & Kudritzki, R. P. 1986, A&A, 164, 86
Poeckert, R. 1981, Pub. Astron. Soc. Pacific, 93, 297
Ramírez-Agudelo, O. H., Sana, H., de Mink, S. E. *et al.* 2015, A&A, 580, A92
Ramírez-Agudelo, O. H., Simón-Díaz, S., Sana, H. *et al.* 2013, A&A, 560, A29
Reese, D. R., Mirouh, G. M., Espinosa Lara, F., Rieutord, M., & Putigny, B. 2021, A&A, 645, A46
Reiners, A., & Royer, F. 2004, A&A, 428, 199
Repolust, T., Puls, J., & Herrero, A. 2004, A&A, 415, 349
Rieutord, M. 2006, A&A, 451, 1025
Rieutord, M. 2016, in Lecture Notes in Physics, vol. 914, 101. 1505.03997
Rieutord, M., Espinosa Lara, F., & Putigny, B. 2016, J. Comp. Phys., 318, 277
Schootemeijer, A., Götberg, Y., de Mink, S. E., Gies, D., & Zapartas, E. 2018, A&A, 615, A30
van Leeuwen, F. 2007, A&A, 474, 653
Vink, J. S., de Koter, A., & Lamers, H. J. G. L. M. 1999, A&A, 350, 181
— 2001, A&A, 369, 574